

# A FACILE WAY TO OPTIMIZE PHOTOELECTRIC PROPERTIES OF SnSe NANOSHEETS VIA SONICATION ASSISTED LIQUID-PHASE EXFOLIATION

Thiet Van Duong<sup>1,\*</sup>, Dung Dinh Nguyen<sup>2</sup>, Hong Tuan Nguyen<sup>2</sup>,  
Nhat Van Pham<sup>3</sup>, Nguyen Xuan Chung<sup>4</sup>, Bac Huu Luong<sup>5</sup>, Hong Ngoc Phan<sup>2,\*</sup>

<sup>1</sup>Graduate University of Science and Technology, Vietnam Academy of Science and Technology,  
18 Hoang Quoc Viet, Cau Giay, Ha Noi, Viet Nam

<sup>2</sup>Center for High Technology Development, Vietnam Academy of Science and Technology,  
18 Hoang Quoc Viet, Cau Giay, Ha Noi, Viet Nam

<sup>3</sup>Department of Advanced Materials Science and Nanotechnology, University of Science and  
Technology Hanoi, Ha Noi, Viet Nam

<sup>4</sup>Department of Physics, Hanoi University of Mining and Geology, Ha Noi, Viet Nam

<sup>5</sup>School of Engineering Physics, Hanoi University of Science and Technology,  
Ha Noi, Viet Nam

\*Email: hongpn82@gmail.com; duongthiet86@gmail.com

Received: 15 January 2022; Accepted for publication: 23 March 2022

**Abstract.** Layer-structured SnSe is known as a potential semiconductive material because it is not toxic, relatively abundant in the earth crust and possess unique electronic, optoelectronic properties. This material is also broadly used for many applications such as photodetector, fire detector, thermoelectric devices, energy storing equipment, etc. Its properties can be tuned by changing fabrication methods. In this work, we report on the process of fabricating SnSe nanosheets (SnSe NSs) in a thin film by using a sonication-assisted exfoliation method and a transferring process of SnSe NSs to a SiO<sub>2</sub>/Si substrate for photoelectric characterization. The properties of fabricated thin film was characterized by X-ray diffraction, Raman spectroscopy, Atomic Force Microscopy, Scanning Electric Spectroscopy and photoelectrical conduction measurement. The obtained results show the optimal exfoliation conditions with a duration of 24 hours and an SnSe NS thickness of 2.5 nm. The highest photoresponsivity is approximate 65 mA W<sup>-1</sup> and response time is found around 0.95 s for the case of 62.5 μm SnSe film's thickness. The photocurrent is approximately linear illumination-intensity dependent with an ideal factor of 0.87 under a constant bias of 2.0V and an excitation wavelength of 450 nm. We introduce a simple method of fabrication and controllable photoelectric properties of SnSe NSs.

**Keywords:** SnSe nanosheets, sonication-assisted exfoliation, photodetector, two dimensional materials.

**Classification numbers:** 2.1.1, 2.5.2, 2.10.2

## 1. INTRODUCTION

Photodetector is an optical-electrical device that converts incident light into electrical signal. It has been broadly applied in scientific study such as image sensing, fire detection, optical communication, safety detection, and phototransistor [1]. SnSe has attracted considerable research due to its great carrier mobility ( $\sim 10^5 \text{ cm}^2 \text{ V}^{-1} \text{ s}^{-1}$ ) whose magnitude is  $\sim 1$ - $2$  orders higher than that of Si and GaAs, high absorption coefficient ( $2 \times 10^4$ – $9.5 \times 10^4 \text{ cm}^{-1}$ ), relatively narrow band gap (1.3 eV and 0.9 eV for indirect- and direct bandgap, respectively), low cost, low toxicity, and stability [1]. Currently, studies on photodetector materials can be divided into two main directions: *i*) special wavelength photodetectors which only respond to a narrow wavelength band; *ii*) broadband wavelength photodetectors which respond to a wide range of wavelengths, from the ultraviolet (UV)- to infrared (IR) region. Two-dimensional semiconductor (2D) SnSe is known as an application of photodetector device for a broadband wavelength. Ho *et al.* reported on SnSe ultrathin films prepared by magnetron sputtering method. The obtained film was highly sensitive to a broad wavelength range in UV-VIS-NIR regions, especially it showed an extremely high sensitivity of  $277.3 \text{ AW}^{-1}$  with the corresponding external quantum efficiency of  $8.5 \times 10^4 \%$  and detectivity of  $7.6 \times 10^{11} \text{ Jones}$  [2]. Yao *et al.* reported that SnSe ultrathin films with  $\text{Bi}_2\text{Te}_3$  electrodes relatively abundant in the earth crust and ideally optoelectronic fabricated by PLD method showed high performance in the UV–VIS–NIR regions, the optimal responsivity in the range between 370 nm and 808 nm reached  $5.5 \text{ AW}^{-1}$  with a relevant external quantum efficiency of 1833 % and a detectivity of  $6 \times 10^{10} \text{ cmHz}^{1/2}\text{W}^{-1}$  [3]. Xu *et al.* found that the flexible SnSe photodetector prepared by sputtering method with an ultrabroad spectral response up to  $10.6 \mu\text{m}$  performed sensitivities of  $0.16 \text{ A W}^{-1}$  and  $1745.5 \text{ A W}^{-1}$  for the wavelengths of 404 nm and 850 nm, respectively [4]. SnSe nanosheets synthesized by facile tip ultra-sonication method performed maximum photoresponsivities of  $1.75 \times 10^4 \text{ A/W}$ ,  $4.63 \times 10^3 \text{ A/W}$ , and  $1.52 \times 10^3 \text{ A/W}$  at wavelengths of 405, 532, and 785 nm, respectively, as reported in [5]. In the work of Zheng *et al.* [6], a photoresponsivity of  $1.0 \times 10^4 \text{ A W}^{-1}$  was obtained for a single SnSe nanowire photodetector synthesized by chemical vapor deposition method. Vertical heterostructures based on orthorhombic SnSe/hexagonal  $\text{In}_2\text{Se}_3$  for high-performance photodetectors synthesized by simple physical vapor deposition (PVD) were reported with a photoresponsivity of  $350 \text{ mA W}^{-1}$  [7]. Most of the fabrication methods have focused on physical vapor phase deposition that requires technical complication and expensiveness. For industrial requirements, fabrication methods with characteristics such as simple fabrication process, low cost and high quality will be the preferred approach. Fabricated 2D nanosheets are one of the important materials for expanding applications in industrial manufacturing, so various methods have been developed such as one-pot synthesis, microwave hydrothermal, Li-intercalation exfoliation, ultrasonic liquid exfoliation and liquid metal synthesis. However, there is a small amount in the fabrication of SnSe nanosheets for high-performance photodetectors.

In this study, we synthesized SnSe nanosheets by sonication-assisted solution-based exfoliation method. The dependence of the photoresponsivity on the thickness of the SnSe films was studied. The photocurrent was linearly dependent on the illuminant power density. This work could open up an application direction for fabricating photodetectors on flexible substrates.

## 2. MATERIALS AND METHODS

### 2.1. Preparation of SnSe NSs

SnSe bulk (99.9 %) was purchased from Sigma-Aldrich. In order to prepare 2D SnSe NSs, the tetrabutylammonium bromide (TBAB) substance used with the role is molecules

intercalation into crystal structure of SnSe. 100 g of TBAB powder was dissolved in 50 mL of DI water, forming a transparent solution under magnetic stirring at room temperature. Next, 0.5 g of SnSe powder was added to the above solution and the mixture was constantly stirred. The solution was transferred to a beaker and sonicated with a 100 W-ultrasonic tip for 12, 24 and 30 hours. The sonication exfoliation process was carried out in an ice bath to avoid oxidation of the SnSe NSs. Then, the dispersed solution was centrifuged at 5000 rpm for 30 min to remove the bulk of residual SnSe. Finally, the dispersive SnSe particles were collected by refiltration, followed by transferring to isopropanol (IPA) solvent at a concentration of 1 mg/mL for further characterization.

## **2.2. Fabrication of SnSe NSs-based photodetector**

Typically, a volume of 3 mL of SnSe NSs solution (0.1 mg/mL) was sprayed to be coated on a 100 nm Au finger electrode using a spraying gun (Airbrush, Richpen 112B, Japan) with a 0.2 mm nozzle diameter, here Ar at a pressure of 2 bar was used as the carrier gas. The finger electrode was fabricated on 300 nm SiO<sub>2</sub>/Si by photolithography (Mask Aligner MDA-400M, M.O Tech). The distance between two adjacent fingers was set to be 2 μm and the total active area was 2x2 cm<sup>2</sup>. The thickness of SnSe NSs was determined using a Dektak 3 Profilometer (Bruker).

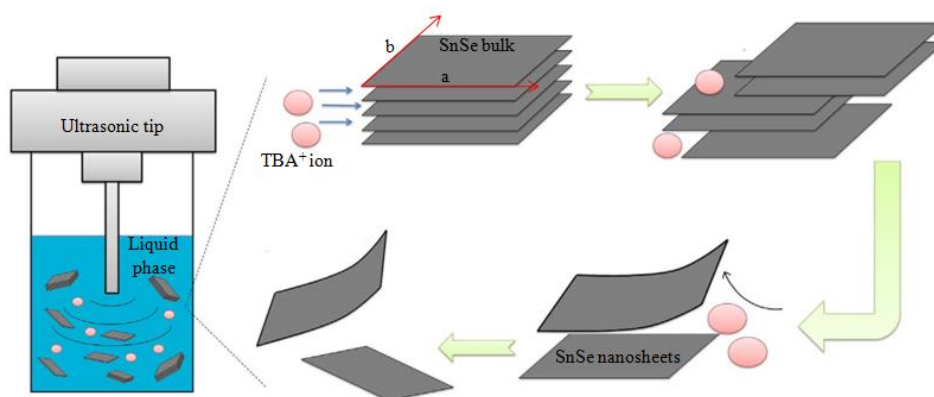
## **2.3. Characterization methods**

The phase purity of bulk SnSe and SnSe NSs was characterized by an X-ray diffractometer with graphite monochromatized Cu K $\alpha$  radiation ( $\lambda = 1.54 \text{ \AA}$ ). Topographic heights of the SnSe NSs deposited on a mica substrate and were characterized using tapping mode of Atomic Force Microscopy (AFM; Veeco, Dimension 3100). Raman spectroscopy was measured from 50 to 2000 cm<sup>-1</sup> at room temperature using a DXR Raman spectrometer with a 532 nm-excitation source (Thermo Scientific). A 500 nm laser-driven tunable light source (LDTLS<sup>TM</sup>, HAMAMATSU) was used for excitation. Sensing performance was characterized in an MST-5000 chamber (MS-Tech) at room temperature. Electronic measurement of the photodetector was carried out by a probe station (Hewlett-Packard-4155A) at room temperature under an applied bias of 2V.

# **3. RESULTS AND DISCUSSION**

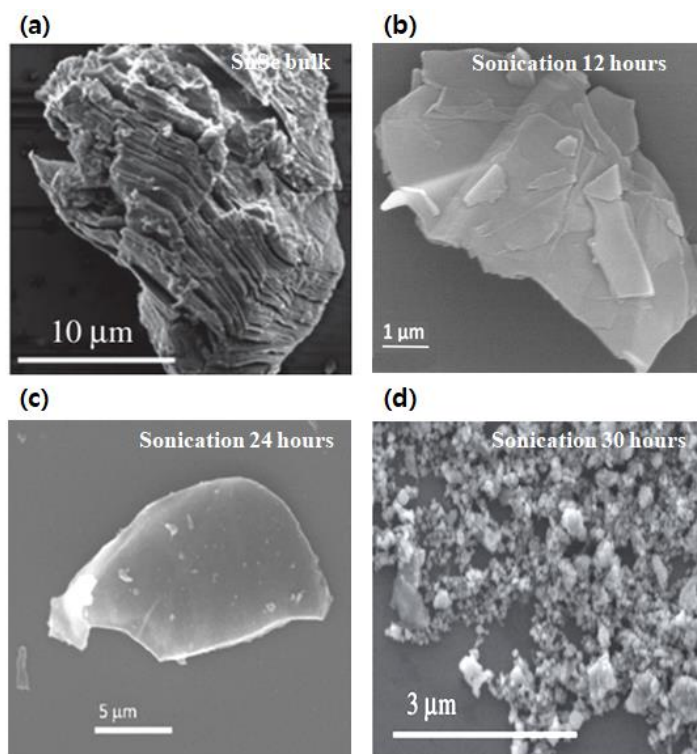
## **3.1. Schematic illustration of synthesis process of SnSe NSs**

Figure 1 shows a synthesis process of SnSe nanosheets based on exfoliation method. Under ultra-sonication conditions, TBAB was intercalated into the SnSe layers along b-c planes as its molecular size is smaller than the distance between two layers along axis a (1.15 nm). During the sonication, agitations cause forceful vibration of individual SnSe layer, more TBA<sup>+</sup> molecules were inserted into the interlayers generating volume expansion inside the SnSe crystal and weakened the layer-layer interaction. As a result of this process, the SnSe layers were efficiently cleavaged, thus leading to the generation of exfoliated SnSe nanosheets.



*Figure 1.* Schematic illustration for TBAB (pink circle) assisted liquid phase exfoliation of SnSe.

### 3.2. Effect of sonication time on morphology of SnSe NSs



*Figure 2.* SEM image of SnSe bulk (a), SnSe nanosheets with various sonication times: 12 hours (b), 24 hours (c) and 30 hours (d).

To optimize the morphology of SnSe NSs, the exfoliation performance was recorded at different times of sonication. Figure 2 shows the morphologies of SnSe bulk and of synthesized SnSe NSs. When the sonication time reaches 24 hours, SnSe NSs exist at the largest size and have uniform lateral size, as shown in Figure 2(c). However, for the sonication time of 12 hours,

SnSe NSs still have agglomeration phenomenon and are broken for the sonication time of 30 hours. This phenomenon proves that the quality of SnSe NSs depends on the sonication time.

### 3.3. The structural and topological characterization of SnSe NSs

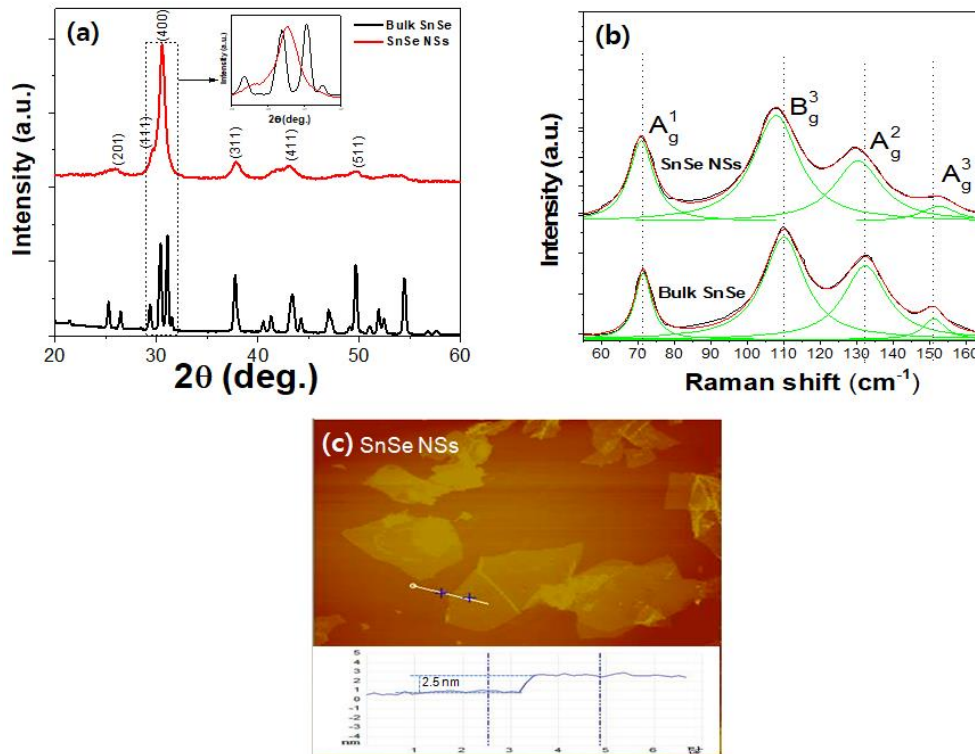


Figure 3. XRD pattern of bulk SnSe and SnSe NSs with sonication time of 24 hours (a), Raman spectra of the SnSe nanosheets (red line) and of SnSe bulk (black line) (b), AFM image of a single SnSe nanosheets and the blue line (in the inset) displays the height profile across the nanosheets (c).

The structure and topology of SnSe NSs fabricated by spin coating SnSe NSs solution (0.5 mg/mL) on a silica substrate were investigated by XRD, Raman scattering and AFM. Figure 3(a) shows the XRD pattern of bulk SnSe and SnSe NSs with sonication time of 24 hours. All diffraction peaks denote the orthorhombic structured SnSe phase ( $Pm\bar{m}a$  space group) with lattice constants of  $a = 11.49$ ,  $b = 4.44$  and  $c = 4.13$  Å (JCPDS no.48-1224). The strongest diffraction peak of  $31^\circ$  was indexed as (400) peak, however, SnSe NSs's peak shifts to lower diffraction angle than bulk SnSe. The downward shift indicates that the volume expansion of SnSe NSs is along a-axis. This can be explained by the intercalation of  $TBA^+$  cations into the crystal structure of SnSe. Figure 3b shows the Raman spectrum of exfoliated SnSe NSs and bulk SnSe with a laser excitation wavelength of 532 nm, and excitation power set at 0.5 mW to avoid damage to the samples. Clearly, the SnSe NSs exhibited four main peaks which are assigned to  $A_g^1$ ,  $B_g^3$ ,  $A_g^2$ , and  $A_g^3$  [8, 9], where the  $A_g^1$  mode is a shear mode along  $a$  axis, shifting atoms out of plane, the  $B_g^3$ ,  $A_g^2$  modes originate from the in-plane shear vibration along  $b$  and  $c$  axes, respectively, the  $A_g^3$  mode corresponds to Sn and Se atoms vibrating out of plane along  $a$  axis. In comparison to bulk SnSe, while the  $B_g^3$  and  $A_g^2$  vibration modes of SnSe NSs show left shift, the right shift is clearly observed in the  $A_g^3$  peak. The  $A_g^3$  phonon mode

corresponds to interlayer interaction along  $a$ -axis which is weakened when the thickness of SnSe decreases. In contrast, the left shift of the  $B_g^3$  and  $A_g^2$  modes may be originated from strengthening interlayer vibration of Sn and Se atoms in  $b$ - $c$  planes which enhance within few layers. All these above evidences demonstrate the high crystal quality of as-synthesized SnSe NSs [10]. In Figure 3(c), the AFM image of SnSe NSs is shown. The thickness of SnSe nanosheets is around 2.5 nm. As reported in the literature, the thickness of a single layer SnSe sheet is about 1 nm [11], hence our synthesized SnSe NSs contain two or three single layers.

### 3.4. Effects of SnSe film thickness on photoelectric properties

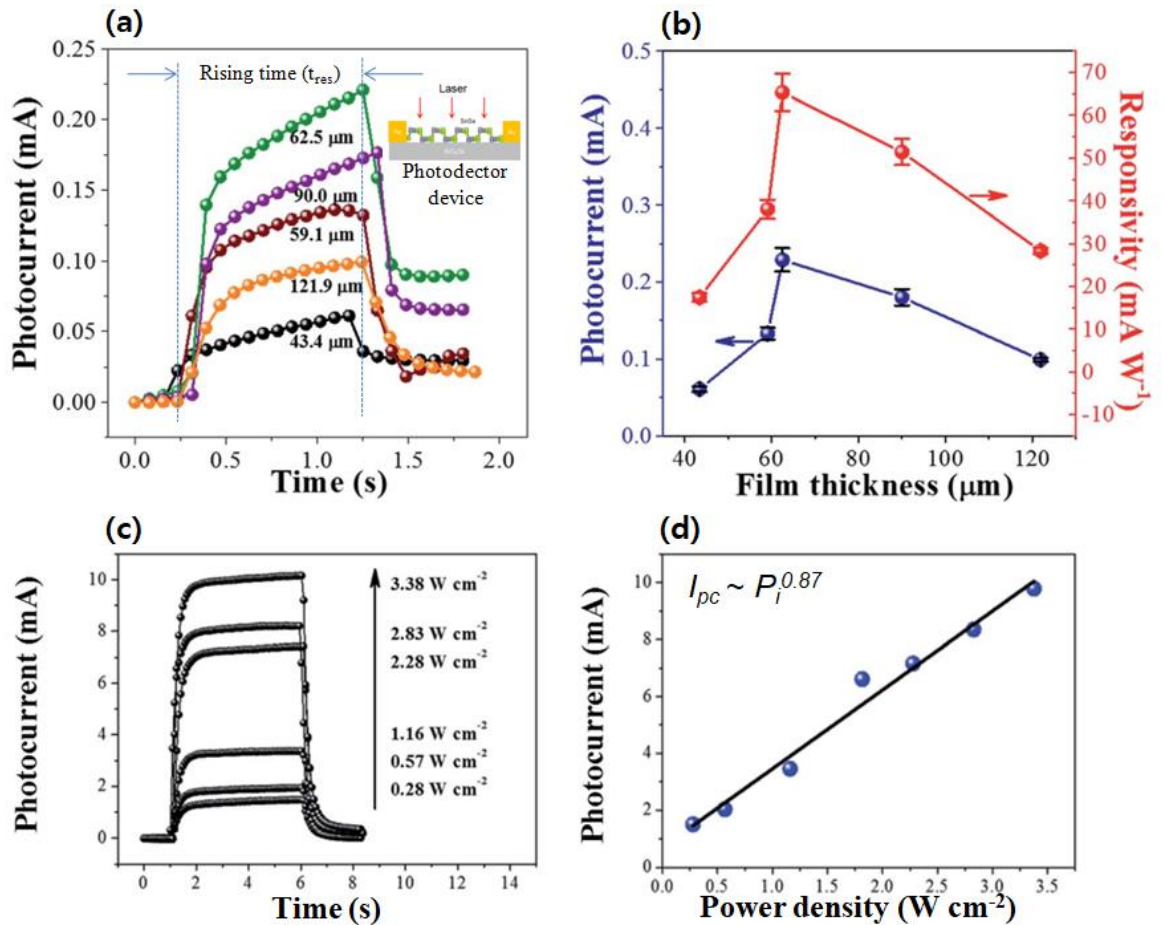


Figure 4. Time-dependence of the photocurrent upon different thicknesses (a); SnSe film's thickness dependence of photocurrent and photoresponsivity (b), time-dependence of the photoresponse of SnSe film's thickness with different laser power densities (c), linear dependence of photocurrent on the incident light power density, under a constant bias of 2.0 V (d).

The inset of Figure 4(a) shows the device structure of the fabricated SnSe NSs photodetector. To demonstrate the device performance, photocurrent generation was under an excitation wavelength of 450 nm generated by a light emitting diode (LED). The excitation photon energy ( $\sim 2.75$  eV) is much higher than the band gap of SnSe, so the photodetector shows the photoresponse in a photoconductor mode. The photocurrent is defined as  $I_{pc} = I_{laser} - I_{dark}$ ,

where  $I_{\text{dark}}$  and  $I_{\text{laser}}$  represent the currents through the photodetector under dark and laser illumination condition, respectively. The laser switches between “on” and “off” states, the device exhibits two current states of “high” and “low”, respectively. Figure 4(a) shows the enlarged response curve of time-dependent photocurrent upon various thicknesses, an excitation laser beam with an intensity of  $1.0 \text{ Wcm}^{-2}$  was applied, the shortest rising time ( $t_{\text{res}}$ ) of  $\sim 0.95 \text{ s}$  with the SnSe NCs thickness of  $62.5 \mu\text{m}$  is found. In this work,  $t_{\text{res}}$  is defined as the time interval for the photocurrent to rise from 10 to 90 % of peak value in each single cycle. The photoresponsivity, which is known as the key parameter for the assessment of the photodetector efficiency, is calculated using the following formula:

$$R(\text{mA W}^{-1}) = I_{pc}(\text{mA})/P_i(\text{Wcm}^{-2}) \times A(\text{cm}^2)$$

where  $I_{pc}$  is the photocurrent generated from the device,  $P_i$  is the incident radiant intensity, and  $A$  is the excited area of the sample. Figure 4(b) shows the photocurrent and photoresponsivity as a function of thickness under an excitation wavelength of  $450 \text{ nm}$  with an illumination intensity of  $1 \text{ Wcm}^{-2}$  and a constant bias of  $2\text{V}$ . When the film thickness varies from  $43.4 \mu\text{m}$  to  $121.9 \mu\text{m}$ , the photoresponsivity rapidly increases then reaches a maximum value of  $65 \text{ mA W}^{-1}$  at a thickness of  $62.5 \mu\text{m}$ , then it slowly goes down. The mechanism for the thickness dependence of photoresponsivity will be further investigated. To estimate the quality of the photodetector device, different values of the excitation power density were applied under a constant bias of  $2\text{V}$  at an SnSe film's thickness of  $62.5 \mu\text{m}$ , as shown in Figure 4(c). Figure 4(d) displays the variation of  $I_{pc}$  as the laser power  $P_i$  increases with a fitted function of  $I_{pc} \propto P_i^\theta$ , where  $\theta$  is an ideal factor. For the photoconductive-type detector,  $\theta$  is usually less than 1. In this study, the obtained ideal factor of 0.87 demonstrates good absorption and good response to the incident laser electron-hole generation in the SnSe channel.

#### 4. CONCLUSION

We have successfully synthesized SnSe NSs using sonication assisted exfoliation method with TBAB as intercalation molecules. The results show the optimal exfoliation conditions with a duration of 24 hours and an SnSe NSs's thickness of  $2.5 \text{ nm}$ . A photodetector device based on SnSe NSs with different thicknesses were successfully fabricated. A maximum photoresponsivity of  $65 \text{ mA W}^{-1}$  and a response time of  $0.95 \text{ s}$  were obtained when the SnSe film's thickness is  $62.5 \mu\text{m}$ . Our work has the potential to design and develop flexible broadband photodetectors based on 2D SnSe layered materials.

**Acknowledgement:** The authors would like to acknowledge the financial support of Graduate University of Science and Technology under the Grant number of **GUST.STS.DT2020-VL02**.

**Credit authorship contribution statement:** Dung Dinh Nguyen designs the experiments, performs some parts of the experiments, prepare figures, Hong Tuan Nguyen and Nhat Van Pham perform some parts of the experiments; Nguyen Xuan Chung and Bac Huu Luong correct the grammar of manuscript and revise manuscript; Hong Phan Ngoc and Thiet Van Duong wrote and revised the manuscript.

**Declaration of competing interest.** The authors declare that they have no known competing financial interests or personal relationships that could have appeared to influence the work reported in this paper.

## REFERENCE

1. Wanga B., Zhong S. P., Zhang Z. B., Zheng Z. Q., Zhang Y. P., Zhang H. - Broadband photodetectors based on 2D group IV<sub>A</sub> metal chalcogenides semiconductors, *Appl. Mater. Today* **15** (2019) 115-138. <https://doi.org/10.1016/j.apmt.2018.12.010>.
2. Hao L., Du Y., Wang Z., Wu Y., Xu H., Dong S., Liu H., Y. Liu, Q. Xue, Z. Han, K. Yan, M. Dong - Wafer-size growth of 2D layered SnSe films for UV-Visible-NIR photodetector arrays with high responsivity, *Nanoscale* **12** (2020) 7358-7365. <https://doi.org/10.1039/D0NR00319K>.
3. Yao J., Zheng Z., Yang G. - All-Layered 2D Optoelectronics: A High-Performance UV-vis-NIR Broadband SnSe Photodetector with Bi<sub>2</sub>Te<sub>3</sub> Topological Insulator Electrodes, *Adv. Funct. Mater.* **2017** (2017) 1701823. <https://doi.org/10.1002/adfm.201701823>.
4. Xu H., Hao L., Liu H., Dong S., Wu Y., Liu Y., Cao B., Wang Z., Ling C., Li S., Xu Z., Xue Q., Yan K. - Flexible SnSe Photodetectors with Ultrabroad Spectral Response up to 10.6 μm Enabled by Photobolometric Effect, *ACS Appl. Mater. Interfaces* **12** (2020) 35250-35255. <https://doi.org/10.1021/acsami.0c09561>.
5. Li X., Song Z., Zhao H., Zhang W., Sun Z., Liang H., Zhu H., Pei J., Li L., Ruan S. - SnSe Nanosheets: From Facile Synthesis to Applications in Broadband Photodetections, *Nanomaterials* **11** (2021) 49. <https://doi.org/10.3390/nano11010049>.
6. D. Zheng, H. Fang, M. Long, F. Wu, P. Wang, F. Gong, X. Wu, J. C. Ho, L. Liao, W. Hu - High-Performance Near-Infrared Photodetectors Based on p-Type SnX (X = S, Se) Nanowires Grown *via* Chemical Vapor Deposition, *ACS Nano* **12** (2018) 7239-7245. <https://doi.org/10.1021/acsnano.8b03291>.
7. Li X. Z., Wang Y. F., Xia J., Meng X. M. - Growth of vertical heterostructures based on orthorhombic SnSe/hexagonal In<sub>2</sub>Se<sub>3</sub> for high-performance photodetectors, *Nanoscale Adv.* **1** (2019) 2606-2611. <https://doi.org/10.1039/C9NA00120D>.
8. Gong X., Wu H., Yang D., Zhang B., Peng K., Zou H. - Temperature dependence of Raman scattering in single crystal SnSe, *Vib. Spectrosc.* **107** (2020) 103034. <https://doi.org/10.1016/j.vibspec.2020.103034>.
9. Chakraborty B., Matte H. S. S. R., Sood A. K., Rao C. N. R. - Layer-dependent resonant Raman scattering of a few layer MoS<sub>2</sub>, *J. Raman Spectrosc* **44** (2013) 92. <https://doi.org/10.1002/jrs.4147>.
10. Lu D., Yue C., Luo S., Li Z., Xue W., Qi X., Zhong J. - Phase controllable synthesis of SnSe and SnSe<sub>2</sub> films with tunable photoresponse properties, *Appl. Surf. Sci.* **541** (2021) 148615. <https://doi.org/10.1016/j.apsusc.2020.148615>.
11. Li L., Chen Z., Hu Y., Wang X., Zhang T., Chen W., Wang Q. - Single-Layer Single-Crystalline SnSe Nanosheets, *J. Am. Chem. Soc.* **135** (2013) 1213-1216. <https://doi.org/10.1021/ja3108017>.